Computational investigations of the reactivity of metalloporphyrins for ammonia oxidation

Melissa Barona,[†] Samantha I. Johnson,*[,†] Margareth Mbea,[§] R. Morris Bullock,[†] and Simone Raugei*[,†]

[†]Center for Molecular Electrocatalysis, Pacific Northwest National Laboratory, Richland, WA 99352, USA

[§] Department of Chemistry, Xavier University of Louisiana, Drexel Dr., New Orleans, LA 70125, USA

KEYWORDS: ammonia oxidation, metalloporphyrins, density functional theory, electrocatalysis, electrochemistry, N-H bond cleavage, N-N bond formation

ABSTRACT: Density functional theory and molecular dynamics simulations were used to assess the ability of tetraphenylporphyrin (TPP)M complexes (where M = Cr, Mn, Fe, Co, Ni, Mo, Ru, W, and Os) to coordinate and weaken the N-H bonds of ammonia, as well as their reactivity towards N-N bond formation for N_2 generation. Compared to other metalloporphyrins, bis-ammonia complexes (TPP)Mo$(NH_3)_2$ and (TPP)W$(NH_3)_2$ exhibit low and level N-H BDFEs due to a stabilized (TPP)M(NH_3)(NH) intermediate by multiple metal-ligand bonding. These results resemble those previously obtained for polypyridyl metal complexes, suggesting that broad trends in reactivity towards N-H bond cleavage are more metal-dependent rather than ligand-dependent for a metal in a nitrogen pseudo-octahedral environment. We investigated N-N bond formation via NH_3 nucleophilic attack on M-NH and M-N intermediates, compared to bimolecular coupling of M-NH_x intermediates. We evaluated the reactivity of (TPP)Fe$(NH_3)_2$ towards N-N bond formation via a hydrazine pathway, and found amide-amide coupling to form a bridged hydrazido complex to be the most favorable pathway for N-N bond formation. Further investigation of possible N-N bond formation pathways by reaction with NH_3 led us to identify a possible Fe^{III}-•NH species with significant aminyl character that bypasses the nucleophilic attack of NH_3 and that promotes homolytic N-H bond cleavage of ammonia. This reaction forms a Fe-NH_2 moiety and a transient •NH_2 radical that subsequently forms an N-N bond with the Fe-NH_2 moiety to form a (TPP)Fe$(NH_3)(N_2H_4)$ species. These results indicate the need to evaluate the radical character of imido species and their reactivity towards N-H bond cleavage of ammonia.

1. Introduction

Ammonia is a promising carbon-free based fuel for storing the power generated by renewable energy technologies to meet increasing energy demand and mitigate climate change.[1-3] Ammonia can be easily liquified and transported using the existing infrastructure developed for the Haber-Bosch process,[2] and the stored energy can be regenerated as electricity in ammonia fuel cells.[4-8] To produce electricity, ammonia can be electrocatalytically oxidized to nitrogen, protons, and electrons (1).[9] Transition metal molecular complexes represent an ideal platform to understand and identify fundamental design principles for electrocatalytic conversion of ammonia to nitrogen. Indeed, the well-defined nature of homogeneous catalysts and the wide range of mechanistic information accessible lend themselves more readily to detailed quantitation of individual reactions from either experiment or modeling than it does for heterogeneous counterparts. In this paper, we report a systematic computational analysis of porphyrin-based metal complexes for ammonia oxidation.

(1)

Conversion of NH_3 to N_2 requires the cleavage of its N-H bonds and subsequent N-N bond formation. N-H bond cleavage can occur electrochemically via sequential proton-coupled electron transfer (PCET) steps,[10-13] or via homolytic N-H bond scission with the use of a radical mediator[11, 14-16] that abstracts an H atom from NH_3 (hydrogen atom abstraction, HAA). The mediator can, in principle, be regenerated electrochemically. The N-H bonds of ammonia are strong, with a first homolytic bond dissociation free energy (BDFE) of 99.4 kcal/mol in the gas phase.[17] When NH_3 coordinates to the metal center of a transition metal complex L_nM (where L_n is the ligand), its N-H bonds can be weakened such that N-H bond cleavage is facilitated.[13]

N-N bond formation has been postulated to occur through the bimolecular coupling of L_nM-NH_x intermediates that result from the N-H bond cleavage reactions (**Scheme 1**).[15, 18-21] In prior work, we investigated computationally the reactivity of poly-pyridyl $[(PY5)M^{II}\text{-}NH_3]^{2+}$ complexes (where M = Cr, Fe, Mo, W, Ru, and Os; and PY5 = 2,6-bis(1,1-bis(2-pyridyl)ethyl)pyridine). We found the molecular complex $[(PY5)Mo^{II}(NH_3)]^{2+}$ favors N_2 production via the coupling of $[(PY5)Mo^{IV}(N)]^{2+}$ nitride intermediates.[18] Recent work by Peters and co-workers demonstrated the stepwise conversion of NH_3 oxidation via the bimolecular coupling of Ni^{III}-NH_2 species that results in a bridged $Ni^{II}(N_2H_4)$ complex.[19] Treatment with the H atom abstractor, tri-*tert*-butylphenoxyl radical (**ArO•**), results in a bridged $Ni^{II}(N_2H_2)$ complex, from which N_2H_2 is released and disproportionates to ½ N_2 and ½ N_2H_4 upon treatment with excess NH_3. We recently achieved catalytic ammonia oxidation with (TMP)$Ru^{II}(NH_3)_2$ (TMP = tetramesitylporphyrin) using the bulkier 2,6-di-tert-butyl-4-tritylphenoxyl radical (**Ph_3C-ArO•**),[15] which hinders the formation of an amine product that can result from C-N coupling reactions with **ArO•**. Our computational investigations of the system, together with prior reports of stochiometric N-N coupling with co-facial Ru porphyrins[22, 23] led us to postulate that N-N bond formation was achieved through the coupling of (TMP)$Ru^{III}(NH_3)(NH_2)$ intermediates.

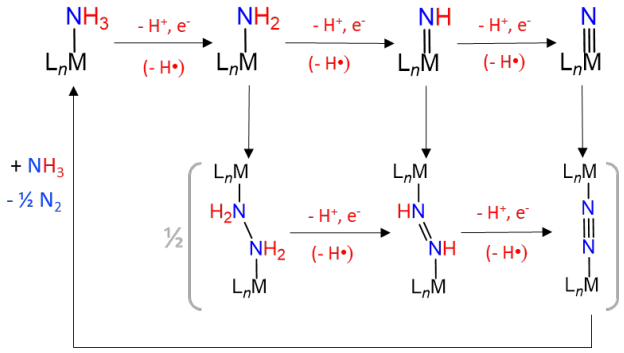

Scheme 1: N-N bond formation and N_2 generation via bimolecular coupling of amide (L_nM-NH_2), imide (L_nM-NH), and nitride (L_nM-N) intermediates

N-N formation may also occur via the addition of NH_3 to M-NH_x intermediates[24-26] (**Scheme 2**). Mock and co-workers[16] demonstrated the catalytic oxidation of NH_3 to N_2 using $[Cp^*Ru(P^{tBu}_2N^{Ph}_2)(NH_3)]^+$, and isotopic labeling studies suggest $^{15}N\equiv{}^{14}N$ formation occurs through attack of $^{14}NH_3$ on a $Ru^{15}NH_x$ (x = 0, 1, or 2) intermediate. Hamann, Smith, and co-workers demonstrated conversion of NH_3 to N_2 using $[Ru(trpy)(dmabpy)(NH_3)]^{2+}$ (where trpy = 2,2′:6′,2″-terpyridine, and dmabpy = 4,4′-bis(dimethylamino)-2,2′- bipyridine). Their experiments suggest that the oxidation reaction proceeds through a $[Ru^{II}\text{-}NH_2NH_2]^{2+}$ intermediate.[27] A prior proposed mechanism for N-N bond formation by nucleophilic attack of a secondary amine on a transient Os^{IV} imido intermediate[25,26] led the researchers to suggest that the $[Ru^{II}\text{-}NH_2NH_2]^{2+}$ intermediate results from NH_3 nucleophilic attack on an undetected Ru^{IV}=NH intermediate.

Motivated by these experimental observations, Najafian and Cundari[28] investigated computationally the electrocatalytic activity of $[Ru(trpy)(dmabpy)(NH_3)]^{2+}$ and its Fe congener towards ammonia oxidation. Their mechanistic studies suggest N-N bond formation via nucleophilic attack by NH_3 on the imido intermediate, along with H transfer to form a hydrazido complex, is more favorable than the alternative N-N bond formation pathway in which NH_3 nucleophilic attack occurs on the nitride complex. Subsequent N-H bond cleavage steps to generate N_2 are lower in energy compared to the M^{II}-NH_3 adduct.

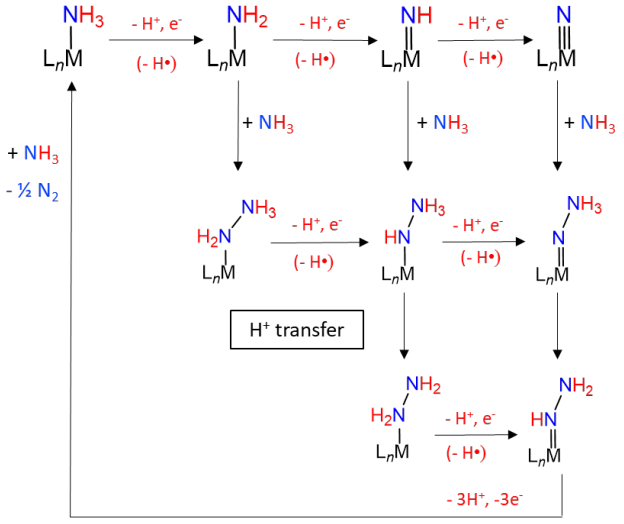

Scheme 2: N-N bond formation and N_2 generation via NH_3 nucleophilic attack on amide (L_nM-NH_2), imide (L_nM-NH), and nitride (L_nM-N) intermediates followed by proton transfer

Additionally, N-N bond formation may occur through intramolecular coupling of adjacent M-NH_x ligands. Peters and coworkers recently achieved electrocatalytic ammonia oxidation to N_2 with $[(bpyPy_2Me)Fe(MeCN)_2]^{2+}$ ($bpyPy_2Me$ = 6-(1,1-bis(pyridin-2-yl)ethyl)-2,2'-bipyridine), for which multiple N-N coupling pathways were proposed.[29] Upon treatment with NH_3, electrochemical data reveal the formation of a $[(bpyPy_2Me)Fe(NH_2)(NH_3)]^{2+}$ complex with adjacent amide and ammine ligands. Computational work suggested that NH_3 nucleophilic attack and subsequent H^+ transfer on Fe-imido and Fe-nitrido intermediates can occur to form Fe-$(NH_3)(N_2H_4)$ and Fe-$(NH_3)(NH\text{-}NH_2)$ intermediates while the adjacent NH_3 ligand remains inactive during the reaction. Alternatively, N-H bond cleavage of the adjacent NH_3 ligand can lead to the formation of a Fe-$(NH_2)(NH_2)$ complex with adjacent amide ligands, which can N-N couple to form a hydrazido complex.

Monometallic N-N bond formation through reaction with NH_3 has several advantages. It can benefit from high NH_3 concentration and facilitate greater control of ligand design when steric hindrance is desired to prevent side reactions with the radical HAA agent.[30] As for bimolecular NH_x-NH_y routes (where x, y > 0), a hydrazine pathway involving NH_3 addition to a M=NH species necessitates a lower net change in oxidation state on the active metal center, which could manifest in lower overpotentials compared to the coupling of terminal nitrido complexes to generate N_2.[30] This mechanism could also lead to $L_nM(N_2H_4)$ species with weaker N-H BDFEs compared to NH_3, which can facilitate N_2 production as observed by Najafian and Cundari.[28] Note that the N-H BDFE of hydrazine in the gas phase is 72.3 kcal/mol[17], 27.1 kcal/mol lower than that of NH_3, and can be further weakened by coordination to the metal center of a transition meal complex.[13]

Inspired by the catalytic activity of $(TMP)Ru^{III}(NH_3)_2$ and seeing to improve our understanding of the reactivity of molecular complexes for ammonia oxidation, we investigated the reactivity of $(TPP)M(NH_3)_2$ (TPP = tetraphenylporphyrin) complexes (where M = Cr, Mn, Fe, Co, Ni, Mo, Ru, W, and Os) using density functional theory (DFT) and molecular dynamics (MD) simulations. We assessed the ability of the metalloporphyrins to weaken the N-H bond of ammonia and their reactivity towards N-N bond formation by NH_3 addition vs. bimolecular NN coupling. We investigated N-N bond formation via a hydrazine pathway for $(TPP)Fe(NH_3)_2$, as iron is a promising earth-abundant metal for the electrocatalytic conversion of NH_3 to N_2. We identified alternative mechanisms via which a $(TPP)M^{II}(NH_2NH_2)$ intermediate could be obtained *en route* to N_2 production by reacting with NH_3, and investigated the possible bimolecular coupling of two $(TPP)Fe(NH_3)(NH_2)$ to form a bridged $Fe^{II}(N_2H_4)$ complex. Understanding the possible mechanisms through which N-N bond formation can occur is essential for learning ways in which transition metal complexes can be tuned and improved for the ammonia oxidation reaction.

2. N-H Homolytic Bond Dissociation Free Energies

Our calculation suggest that HAA occurs on both NH_3 ligands of $(TMP)Os(NH_3)_2$ resulting in the formation of a $(TMP)Os(NH_2)_2$ complex that showed no evidence for N-N bond formation.[31] Because HAA can theoretically occur from both NH_3 ligand, we calculated all possible HAA for $(TPP)M(NH_3)_2$ complexes until the metal center reaches its highest accessible oxidation state (**Figure S1**). When considering only HAA energetics, HAA from a single NH_3

molecule leading up to (TPP)M(NH_3)(N) is the most favorable pathway for all complexes except for (TPP)Os(NH_3)$_2$, which favor the formation of (TPP)M(NH_2)$_2$ complexes. Although HAA from the *trans* NH_3 ligand of (TPP)Os(NH_3)(NH_2) is favored over HAA to form the imido intermediate (TPP)Os(NH_3)(NH), subsequent HAA for the bis-amido complexes is appreciably disfavored; the sequential removal of H atoms from the same NH_3 ligand is the most favored pathway (**Figure S1**).

To assess the ability of the (TPP)M complexes to weaken the N-H bonds of ammonia, we first examined the N-H BDFEs associated for HAAs from a single NH_3 ligand leading up to the nitrido intermediates (**Figure 1**). N-H BDFEs are referenced to the O-H BDFE of the tri-tert-butyl phenol (ArOH) molecule in benzene, which is 76.7 kcal/mol.[17]

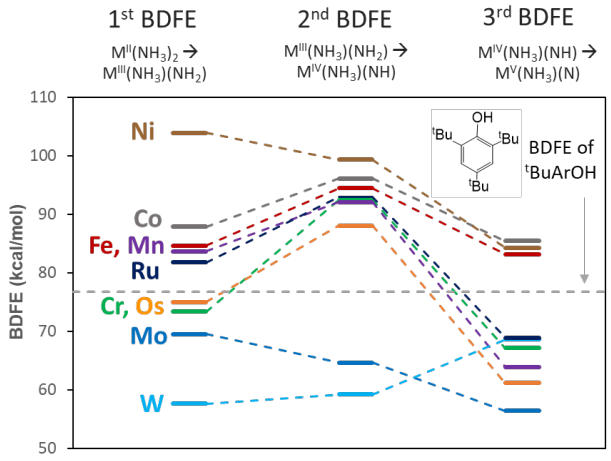

Figure 1: (a) 1st, 2nd, and 3rd BDFEs of (TPP)M(NH_3)$_2$ complexes to form (TPP)M(NH_3)(N). Values are tabulated in Table S5.

The first N-H BDFE values range from 57.7 (W) to 103.9 kcal/mol (Ni). W, Mo, Cr, and Os porphyrins exhibit first BDFE values lower than that of the ArO-H bond, indicating thermodynamically favorable HAA and coordination-induced N-H bond weakening by these metals. Mo and W porphyrins particularly show low and level BDFEs because of the lower second BDFE values compared to the rest of the metals. The lowering of the second BDFE results from the stabilization of their respective imido intermediates. Structural analysis of (TPP)Mo(NH) and (TPP)W(NH) reveals that the complexes adopt a C_{4v} symmetry and linear M-N-H moieties, resembling the behavior of the computationally studied (PY5)Mo and (PY5)W complexes reported by our group.[18] Electronic structure analysis within the natural bond orbital (NBO) framework[32] reveals multiple metal ligand bonding[33] within the linear Mo and W imido intermediates. In their formal oxidation state of +IV, Mo and W exhibit a low spin d^2 configuration (**Figure S3**), making their d_{xz} and d_{yz} orbitals available for π bonding. As a result, the second HAA is facilitated by the stabilization of the imido intermediate through a M≡N triple bond (**Figures S9** and **Figure S11**). In contrast to Mo and W, the d electrons of the other metals populate the π* orbital with d_{xz} and d_{yz} contributions within the metal-imido moiety, resulting in weaker M-N bonding interaction, a bent M-N-H geometry, and higher 2nd N-H BDFE values (**Figures S4-S8**, **S10**, and **S12**). Given that similar trends in BDFE values have been observed in our previous investigation of (PY5)M(NH_3)]$^{2+}$ complexes and the [^{NMe3}(bpy)(tpy)M(NH_3)$_2$]$^{2+}$ complexes studied by Najafian and Cundari, these observations indicate that trends in N-H bond cleavage are dependent on the metal rather than dependent on the ligand for a metal in a nitrogen pseudo-octahedral environment.

A less thermodynamically feasible second HAA (as observed for all metals except Mo and W) can facilitate competing pathways, such as N-N coupling of amide intermediates, C-N coupling with ArO•, or HAA from the trans NH_3 ligand. For instance, our computational and experimental work on (TMP)Ru(NH_3)$_2$[15] show that C-N coupling with ArO• to form an amine is favored over further HAA to form the imido intermediate. Catalytic ammonia oxidation to N_2 was achieved with a bulkier phenoxyl radical that hinders the C-N coupling reaction, leading us to postulate that ammonia oxidation occurs via the N-N coupling of (TMP)Ru^{III}(NH_3)(NH_2) intermediates. The reactivity of (TMP)Ru(NH_3)$_2$ differs from that observed for its Os analogue. In the case of (TMP)Os(NH_3)$_2$, HAA from both NH_3 ligands resulted in the formation of a (TMP)Os^{IV}(NH_2)$_2$ complex that was inactive towards N-N coupling and C-N coupling.

The third BDFE is lowest for Mo, W, Cr, Mn, Os and Ru porphyrins. NBO analysis of the (TPP)M(NH_3)(N) complexes (**Figures S13-S14** and **S18-S21**) reveals a M≡N triple bond for these porphyrin complexes, which stabilizes the nitrido intermediate to a greater extent compared to the Fe, Co, and Ni porphyrins. Indeed, in the case of (TPP)Fe(NH_3)(N) and (TPP)Co(NH_3)(N), weaker M-N interactions are found consisting of a double bond for Fe and a single bond for Co (**Figure S15-S16**). Because of the difficulty of Ni to achieve an oxidation state of +V, an ionic interaction between Ni and the N atom in (TPP)Ni(NH_3)(N) takes place instead (**Figure S17**).

In comparison to the [(PY5)M(NH_3)]$^{2+}$ complexes, the BDFE values for the formation of the nitride intermediate are generally lower for the (TPP)M(NH_3)$_2$ complexes by 2-10 kcal/mol, with the exception of the first BDFE of (TPP)Cr(NH_3)$_2$ and (TPP)Mo(NH_3)$_2$ (higher by 8.5 and 1.5 kcal/mol, respectively) and the second and third BDFEs of (TPP)W(NH_3)$_2$ (higher by 4.3 and 1.6 kcal/mol, respectively), and the third BDFE of (TPP)Ru(NH_3)$_2$ (higher by 3.4 kcal/mol). Compared to the [(bpy)(tpy)Ru(NH_3)$_2$]$^{2+}$ and [^{NMe3}(bpy)(tpy)Ru(NH_3)$_2$]$^{2+}$ systems studied by Najafian and Cundari, the (TPP)Ru(NH_3)$_2$ exhibits BDFE values 0.6 to 6.9 kcal/mol higher. Similarly, (TPP)Fe(NH_3)$_2$ exhibits BDFE values 2.6 and 4.1 kcal/mol higher than those reported for [^{NMe3}(bpy)(tpy)Fe(NH_3)$_2$]$^{2+}$ (**Figure S2**). While broad trends in N-H BDFEs are shown to be largely metal dependent in the nitrogen pseudo-octahedral environment, this comparison shows that there is some fine tuning can be achieved by changing the ligand.

3. N-N bond formation via NH_3 addition

Molecular dynamics simulations of representative (TPP)M(NH_3)$_2$ complexes (M = Fe, Ru, and Os) at a typical experimental concentration (0.7 mM) in liquid benzene saturated with ammonia ([NH_3] = 9.5 mM) revealed that at

least one NH_3 is either in the vicinity of or hydrogen bonded to each NH_3 ligand, with an average distance of 3.4 Å between the nitrogen atoms of the NH_3 ligand and the free NH_3 molecule. The results of these simulations are detailed in the Supporting Information. Based on these findings, we next investigated possible mechanisms via which N-N bond formation can occur by direct reaction of $M(NH_x)$ intermediates with NH_3. In this section, we first briefly describe the mechanisms that were investigated to facilitate the subsequent discussion of the results.

The first mechanism we investigated is N-N bond formation through a NH_3 nucleophilic attack. Nucleophilic attack of NH_3 can occur on the amide, imide, or nitride intermediates formed after HAA. Because the amide lacks the necessary electrophilicity to accept electron density, any attempt to locate a stable NH_3 adduct to the $Os(NH_2)_2$ intermediate and the amide intermediate for the rest of the metals failed. Therefore, we investigated N-N bond formation via NH_3 nucleophilic attack on the imide and nitride intermediates. Because $(TPP)Os(NH_3)_2$ favors bis-amide formation, we focused on the rest of the $(TPP)M(NH_3)_2$ structures that favor imide and nitride formation. Nucleophilic attack on $(TPP)M(NH_3)(NH)$ can compete with HAA to form $(TPP)M(NH_3)(N)$, and we assessed trends in these energetics across metals (**Figure 2a**).

Upon NH_3 attack on the imido species, proton transfer can occur from the distal nitrogen atom to the proximal nitrogen atom to form a hydrazido species (**Figure 2a**). The high energetic cost associated with NH_3 nucleophilic attack on an imido intermediate and subsequent proton transfer to form a hydrazido species can be bypassed by a concerted pathway in which proton transfer and N-N bond formation occur synchronously (**Figure 2b**). We investigated this pathway for $(TPP)Fe(NH_3)_2$. This choice was motivated by the considerable interest in Fe complexes for ammonia oxidation,[21, 29, 34] as iron is a promising alternative to using precious metals such as Ru for catalysis, and Fe complexes have been demonstrated to be active towards electrocatalytic ammonia oxidation.[29, 34] In our search for such a mechanism, we additionally identified an alternate pathway in which N-H bond cleavage of NH_3 can occur if there is significant amidyl radical character[35] on the $(TPP)Fe(NH_3)(NH)$ intermediate. This reaction results in the transient formation of a high-energy intermediate consisting of an amide species and an $\bullet NH_2$ moiety that is stabilized by hydrogen bonding between the nitrogen atom of the amido moiety and the H atom of the $\bullet NH_2$. N-N bond formation then occurs as the $\bullet NH_2$ breaks free of the hydrogen bond and attacks the N atom of the amido moiety, forming the hydrazido intermediate (**Figure 2c**).

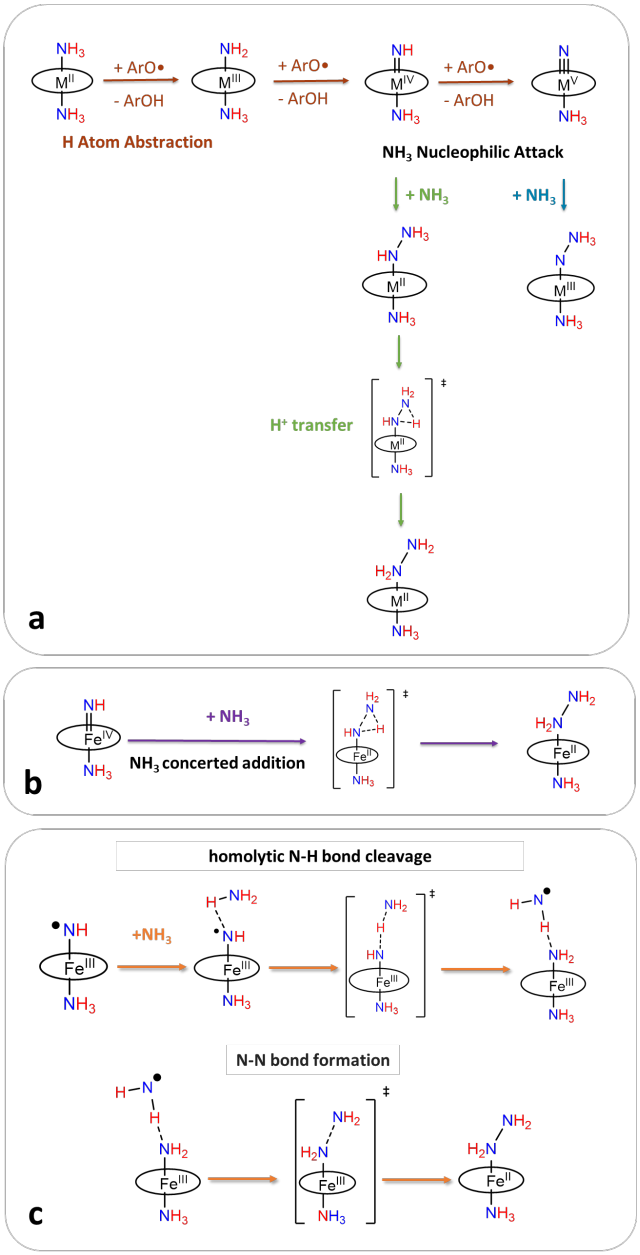

Figure 2: (a) HAA and N-N bond formation by NH_3 nucleophilic attack on the imido species, followed by proton transfer to form a hydrazido. Alternatively, NH_3 nucleophilic attack can occur on the nitride species. (b) N-N bond formation by concerted addition of NH_3. (c) N-H bond homolytic cleavage of NH_3 followed by N-N bond formation between $\bullet NH_2$ radical and Fe-NH_2 moiety. Dashed lines in transition state structures represent bond-making and bond-breaking events. All other dashed lines represent hydrogen bonding.

3.1 N-N bond formation via NH_3 nucleophilic attack

In the case of Cr, Mn, Mo, and W, HAA to form $(TPP)M(NH_3)(N)$ is favored over NH_3 nucleophilic attack on $(TPP)M(NH_3)(NH)$ by a range of 24.3 (Cr) to 67.7 kcal/mol (W) (**Figure 3**). In particular, the free energy for the NH_3 nucleophilic attack on $(TPP)Mo(NH_3)(NH)$ and $(TPP)W(NH_3)(NH)$ are drastically higher (66.2 and 67.7 kcal/mol) than HAA to the nitride due to the triple bond M-

NH interaction that stabilizes the imido intermediate. The formation of multiple metal-ligand bonds in (TPP)M(NH_3)(N) (where M = Cr, Mn, Mo, and W) favors further HAA over NH_3 nucleophilic attack to form (TPP)M(NH_3)(N), and hinders the binding of NH_3, as evidenced by the large positive free energies, ranging from 34.8 (Cr) to 59.1 kcal/mol (Mo) (Table S10).

The Fe, Co, and Ni porphyrin analogues exhibit lower reaction free energies for NH_3 binding to their imide and nitride intermediates due to their weaker M-N bonds. In the case of the Fe porphyrin, NH_3 binding to the imide and nitride intermediates are both 8.1 kcal/mol uphill. In the case of the Co porphyrin, they are 7.2 kcal/mol and 12.3 kcal/mol uphill (**Figure 4**). The nucleophilic attack of ammonia on the imide intermediate is nearly energetically equivalent to HAA to form the nitride intermediate for Fe and Co. In the case of the Ni porphyrin, NH_3 nucleophilic attack on (TPP)Ni(NH_3)(NH) is favored over HAA to form (TPP)Ni(NH_3)(N) by 21.5 kcal/mol as the M-N moiety in (TPP)Ni(NH_3)(N) is highly unstable with no M-N bonding interaction (**Figure S17**).

3.2 M-nitrido vs. M-hydrazido formation

Upon NH_3 binding to the imide intermediate, proton transfer can occur and result in the formation of a hydrazido intermediate, (TPP)M(NH_3)(NH_2NH_2) (**Figure 2a**). As shown in **Figure 3**, (TPP)M(NH_3)(N) formation is favored over the formation of (TPP)M(NH_3)(NH_2NH_2) for Cr, Mo, and W by a range of 3.3 kcal/mol (Cr) and 51.9 kcal/mol (W). DFT calculations indicate that the energetic cost to form (TPP)Mn(NH_3)(N) (free energy change associated with (TPP)Mn(NH_3)$_2$ + 3ArO• + NH_3 → (TPP)Mn(NH_3)(N) + 3ArOH + NH_3) and the energetic cost to form (TPP)Mn(NH_3)(NH_2NH_2) (free energy change associated with (TPP)Mn(NH_3)$_2$ + 3ArO• + NH_3 → (TPP)Mn(NH_3)(NH_2NH_2) + 2 ArO• + 2ArOH) differ within DFT error by 2.1 kcal/mol, suggesting that they could both be thermodynamically accessible. (TPP)M(NH_3)(NH_2NH_2) is favored over (TPP)M(NH_3)(N) by 25.3, 34.0, and 50.8 kcal/mol for the Fe, Co, and Ni analogues, respectively. Given the lower overall free energy change to form (TPP)Fe(NH_3)(NH) compared to the Co and Ni analogues, we investigated further the N-N bond formation via a hydrazine pathway for (TPP)Fe(NH_3)$_2$. Proton transfer (**Figure S47**) to form (TPP)Fe(NH_3)(NH_2NH_2) has a barrier of 29.6 kcal/mol (**Figure 4**). Note that the overall free energy associated with the formation of a hydrazido species, and 2 ArOH molecules is just 7.0 kcal/mol uphill when referenced to (TPP)Fe(NH_3)$_2$, 2 molecules of ArO•, and NH_3. (**Figure 3a**). A mechanism that bypasses the nucleophilic attack of ammonia and the high energy requirement of proton transfer would make N-N bond formation via a hydrazido intermediate a promising pathway towards N_2 formation. In the pursuit of finding such a mechanism, we explored the possibility of a concerted pathway in which N-N bond formation and proton transfer occur simultaneously to form the hydrazido intermediate.

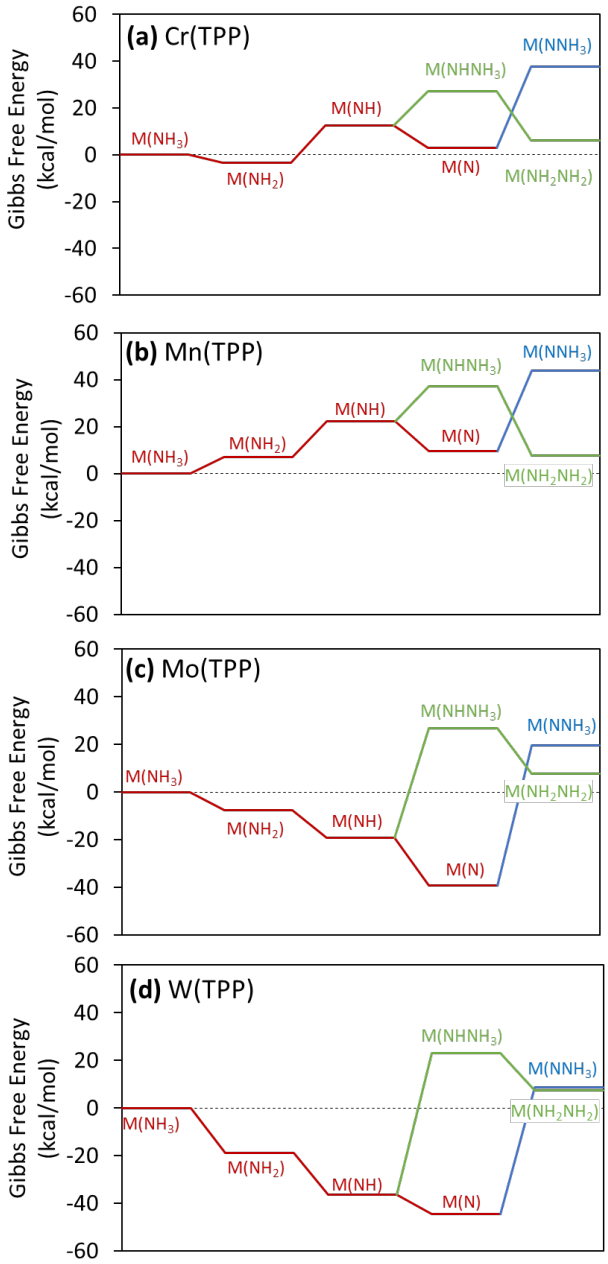

Figure 3: HAA reactions by ArO• [M(NH_x) + ArO• → M(NH_{x-1})+ ArOH] are shown in red, NH_3 nucleophilic attack on the imido intermediate [M(NH) + NH_3 → M($NHNH_3$)) followed by proton transfer to form the hydrazido intermediate [M(NH)(NH_3) → M(NH_2NH_2)] is shown in green, and NH_3 nucleophilic attack on the nitride intermediate [(TPP)M(NH_3)(N) + NH_3 → (TPP)M(NH_3)(NNH_3)] is shown in blue for (a) (TPP)Cr(NH_3)$_2$, (b) (TPP)Mn(NH_3)$_2$, (c) (TPP)Mo(NH_3)$_2$, and (d) (TPP)W(NH_3)$_2$. Free energies are in benzene. The reader is referred to **Figure 2a** for the reaction pathways. The addition of ArO•, and NH_3, and production of ArOH upon HAA are not shown for clarity. Energy pathway values can be found in Section S4 of the Supporting Information. For all these systems, (TPP)M(NH_3)(N) formation is favored over NH_3 nucleophilic on (TPP)M(NH_3)(NH).

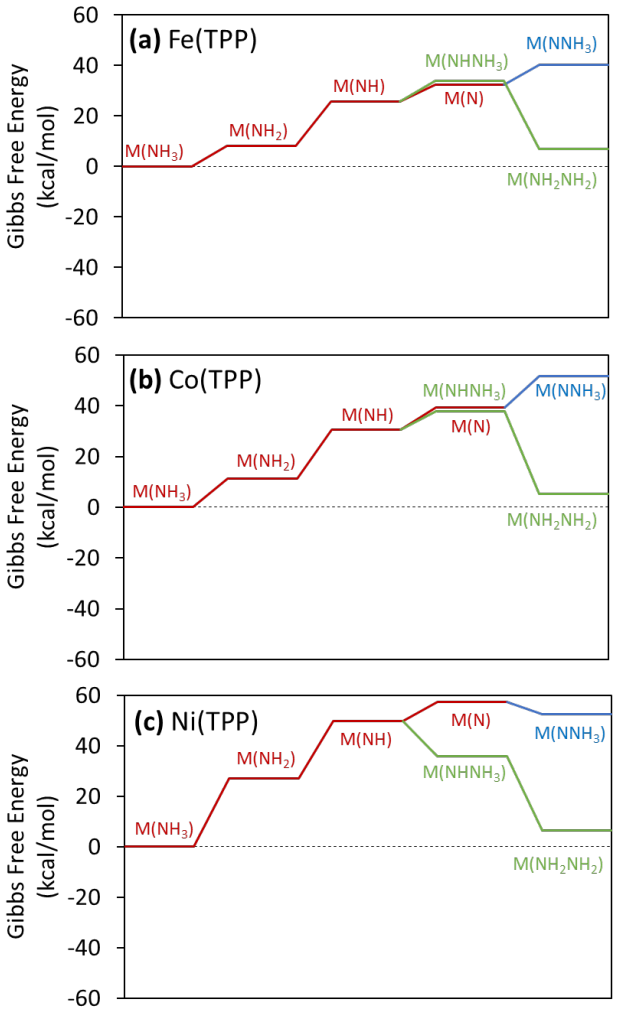

Figure 4: HAA reactions by ArO• [$M(NH_x)$ + ArO• → $M(NH_{x-1})$ + ArOH] are shown in red, NH_3 nucleophilic attack on the imido intermediate [M(NH) + NH_3 → $M(NHNH_3)$] followed by proton transfer to form the hydrazido intermediate [$M(NH)(NH_3)$ → $M(NH_2NH_2)$] is shown in green, and NH_3 nucleophilic attack on the nitride intermediate [$(TPP)M(NH_3)(N)$ + NH_3 → $(TPP)M(NH_3)(NNH_3)$] is shown in blue for (a) $(TPP)Fe(NH_3)_2$, (b) $(TPP)Co(NH_3)_2$, (c) $(TPP)Ni(NH_3)_2$. Free energies are in benzene. The reader is referred to Figure 2a for the reaction pathways. The addition of ArO•, and NH_3, and production of ArOH upon HAA are not shown for clarity. Energy pathway values can be found in section S4 of the Supporting Information. For all these complexes, $(TPP)M(NH_2NH_2)$ formation is favored over $(TPP)M(NH_3)(N)$ formation.

3.3 Fe-hydrazido formation

Prior to studying the formation of a hydrazido intermediate via an alternative pathway, we used MD simulations to investigate the interaction between ammonia and the imide intermediate in the presence of benzene and found that at least one NH_3 molecule is in the vicinity of the imido ligand. Inspection of the MD trajectories revealed that the H atom of the NH_3 molecule can approach as close as 2.5 Å to the N atom of the imido ligand, suggesting hydrogen bonding could occur. However, this interaction is very weak (Tables S13 – S15). Following this observation, we optimized the structure of $(TPP)Fe(NH_3)(NH)$ with the imido moiety as a hydrogen acceptor from the NH_3 molecule (**Figure S45**), and found this interaction energy to be 4.7 kcal/mol uphill. Along with the DFT results, the MD simulations suggest that the formation of a hydrogen bond between ammonia and the imido ligand is not thermodynamically favorable (Table S20).

Nudged Elastic Band (NEB) calculations[36, 37] identified two alternative pathways for the formation of $(TPP)Fe(NH_3)(NH_2NH_2)$ (**Figures 2b** and **2c**). The first pathway is a concerted N-N and N-H bond formation (**Figure 5a**) on the singlet spin state potential energy surface (PES) with an energy barrier of 19.6 kcal/mol (**Figure 6**). We note that the lowest-energy spin state for the imido intermediate is the triplet state. To undergo a concerted mechanism, the imido intermediate must overcome an energy penalty of 9.3 kcal/mol to acquire the restricted singlet spin state.

The second pathway is a two-step process on the triplet spin state PES. The first step is the homolytic N-H bond cleavage by the Fe-imido intermediate (**Figure 5b**) with a reaction barrier of 15.7 kcal/mol. This process results in a $Fe\text{-}NH_2$ moiety and an $•NH_2$ radical that is stabilized by hydrogen bonding with the N atom of the $Fe\text{-}NH_2$ moiety (**Figure S50**). The $•NH_2$ radical then breaks free of the hydrogen bond to form an N-N bond with the $Fe\text{-}NH_2$ moiety (**Figure 5c**) and form the hydrazido complex, overcoming an energy barrier of 6.8 kcal/mol.

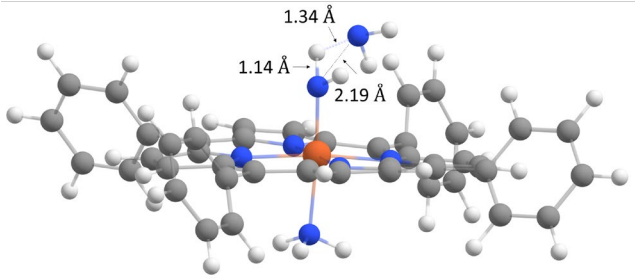

(a)

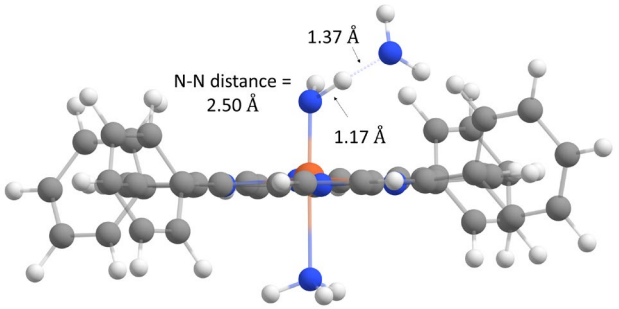

(b)

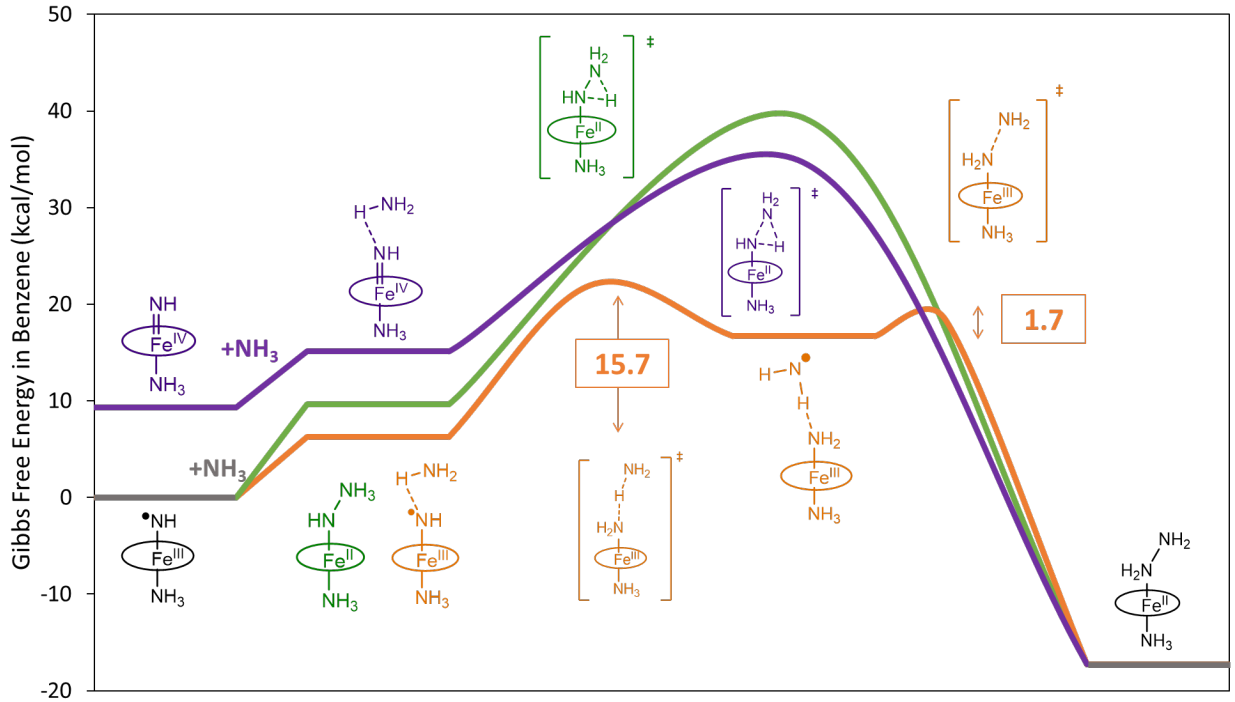

Figure 6: Hydrazido formation via NH_3 nucleophilic attack, followed by H transfer (green), via a concerted pathway in which N-H bond cleavage and N-N bond formation occur synchronously (purple), and via N-H bond cleavage, followed by N-N bond formation (orange). Dashed lines in transition state structures represent bond-making and bond-breaking events. All other dash lines represent hydrogen bonding.

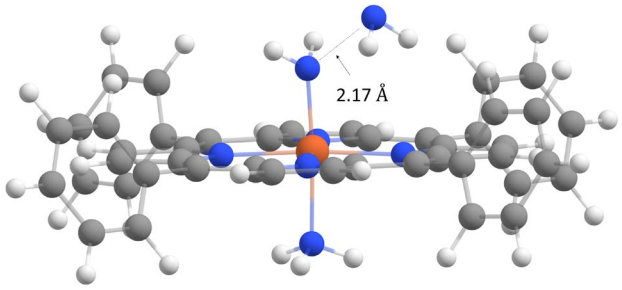

(c)

Figure 5: Transition state structure of (a) concerted N-H bond cleavage and N-N bond formation and (b) homolytic N-H bond cleavage followed by (c) N-N bond formation.

A closer examination of the triplet state of (TPP)Fe(NH_3)(NH) reveals imidyl radical character on the N atom with an NBO spin density of 0.97, suggesting a Fe^{III}-•NH moiety (**Figure 7a** and **Figure S51**). Due to the significant spin density on the N atom of (TPP)Fe(NH_3)(NH), we also investigated this pathway on the open-shell singlet PES, in which the spin on the N is antiferromagnetically coupled with the spin on the Fe center (**Figure S49**). Our results the triplet state of the imido intermediate is lower in energy by ~3 kcal/mol, and that of the transition state and •NH_2 adduct (for which the spin on the •NH_2 is antiferromagnetically coupled with the spin on Fe) are energetically equivalent to the open-shell singlet state. N-N bond formation on the open-shell singlet PES then proceeds through a barrier of just 1.7 kcal/mol, 5.1 kcal/mol lower in energy compared to triplet state. This indicates that spin crossing occurs during N-N bond formation to form the hydrazido species (**Figure S49b**).

Figure 6 compares the three different pathways identified for N-N formation via a hydrazido intermediate, indicating that the most favorable pathway are the sequential N-H bond cleavage and N-N bond formation steps. We suggest that the radical character of the Fe^{III}-•NH moiety favors N-H bond cleavage of NH_3 rather than nucleophilic attack by ammonia followed by proton transfer or NH_3 addition via a concerted mechanism. Homolytic N-H bond cleavage bypasses the high-energy intermediate associated with the nucleophilic attack of NH_3 and presents a viable pathway via which N-N bond formation can occur. In addition, preliminary results on the analogous (TPP)Mn(NH_3)(NH) intermediate reveal an amidyl radical character of -0.79 that exhibits a barrier of 19.4 kcal/mol towards N-H bond homolytic cleavage (Figure S58). These results suggest the need to inspect the radical character of imido species and their reactivity towards N-H bond cleavage of ammonia.

4. N-N bond formation via bimolecular coupling

In our prior work on $[(PY5)M(NH_3)]^{2+}$,[18] we found the free energy change associated with the generation of N_xH_y products to be a good proxy for M-NH_x bimolecular coupling energetics. To assess the overall energetics for the generation of N_xH_y products via bimolecular coupling, we calculated the free energy associated with the release of N_2H_4, N_2H_2, and N_2, and regeneration of the ammonia-bound starting complex from two amido, two imido, and two nitrido intermediates:

$$2\ (TPP)(M)(NH_3)(NH_2) + 2NH_3 \rightarrow 2\ (TPP)M(NH_3)_2 + N_2H_4 \quad (2)$$

$$2(TPP)(M)(NH_3)(NH) + 2NH_3 \rightarrow 2\ (TPP)M(NH_3)_2 + N_2H_2 \quad (3)$$

$2(TPP)(M)(NH_3)(N) + 2NH_3 \rightarrow 2\ (TPP)M(NH_3)_2 + N_2$ (4)

When compared to HAA energetics, further HAA is favored over release of N_2H_4 or N_2H_2 for the Mo and W analogues (**Figure S52**). HAA from the axial NH_3 ligand to form a bis-amide complex is favored over N_2H_4 release for the Ru and Os analogues (**Figure S53**). In the case of the first-row metals, N_2H_4 release becomes more favorable over HAA to form the imido species periodically (**Figure S54**). For instance, compared to HAA to form the imido species, N_2H_4 release is more unfavorable for only the Cr analogue, is nearly energetically equivalent for the Mn and Fe analogues, and is more favorable for Co and Ni. This observation, in particular for Ni, is reminiscent of the experimental work by Peters and co-workers, who demonstrated the bimolecular coupling of Ni^{III}-NH_2 species that resulted in a bridged $Ni^{II}(N_2H_4)$ complex and subsequent release of N_2H_4 and disproportionation to N_2H_2.[19]

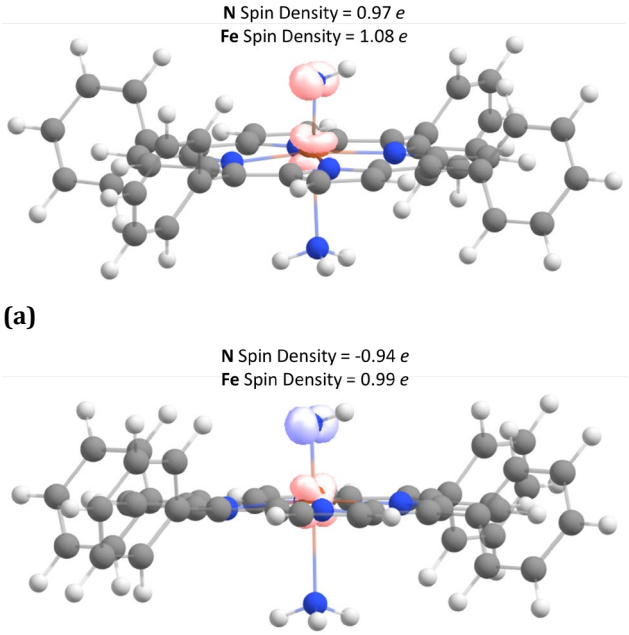

Figure 7: NBO spin density plot (isovalue = 0.05) for the (a) triplet state and (b) open-shell singlet state of (TPP)Fe(NH_3)NH.

N_2H_2 release is more favorable than further HAA to form the nitride species for all first-row metals. Overall, N_2 release is more favorable than N_2H_4 and N_2H_2 release, and the most favorable for the porphyrin analogues containing later transition metals such as Fe, Co, and Ni, which exhibit a weaker metal-nitrido interaction. Note, however, that nitride formation is drastically uphill for these metalloporphyrins (32.3 – 57.4 kcal/mol with respect to the bis-ammonium complex and 3 ArO• molecules) and thus, alternative pathways to nitride-nitride coupling are plausible for N_2 generation. Similar observations were made in our previous investigation of $[(PY5)M(NH_3)]^{2+}$ complexes.

While nitride-nitride coupling may not be the most plausible path towards N_2 generation for some of the porphyrin analogues, it is informative to assess the mechanism through which nitride-nitride coupling may occur, and compare with our previous work on the $[(PY5)M(NH_3)]^{2+}$ complexes.[18] Depending on the nature of the metal-nitrido moiety, nitride-nitride coupling can occur via radical coupling[14] or homocoupling.[38, 39] Radical coupling involves the coupling between two metal-nitridyls, and homocoupling occurs between two ambiphilic nitrides. An ambiphilic nitride has a lone pair on the nitrogen atom of the metal-nitrido moiety and can take the role of an electrophile or nucleophile as it approaches the other nitride intermediate. As the two nitride intermediates couple, one nitride behaves as a nucleophile and donates electron density into the π^* orbital of the other such that the M-N bond breaks and N-N bond formation occurs. In our prior work on $[(PY5)M(NH_3)]^{2+}$ complexes, we found nitride-nitride coupling to be related to the electrophilicity of metal-nitride moieties. The more localized the π^* orbital is on the nitride ligand, the higher the electrophilicity of the M-N bond and the more favorable nitride-nitride coupling.

To assess the reactivity of the (TPP)M(NH_3)(N) intermediates towards nitride-nitride coupling, we opted to use the N_2 generation reaction energies (equation 4) due to the high computational cost required for calculating the bridged N_2 structures at the level of theory used in this work. In our work on $[(PY5)M(NH_3)]^{2+}$, we found these energies to correlate well with the nitride-nitride coupling reaction energy. We assessed the electrophilicity of the metal-nitrido by calculating the fraction of the π^* orbital on the nitrido using NBO analysis. **Figures S56-S58** shows the correlation between the N_2 generation reaction energies and the electrophilicity of the M-N ligand. We omit (TPP)Co(NH_3)(N) and (TPP)Ni(NH_3)(N) from this analysis as they lack a π bond interaction between the metal and the N (**Figures S16** and **S17**). These results suggest that as the electrophilicity of the M-N ligand increases, the more favorable N_2 generation becomes. Along with our observations $[(PY5)M(NH_3)]^{2+}$ systems, these results further corroborate the need for an electrophilic M-N π bond for nitride-nitride coupling granted that a nitride ligand can be formed electrochemically or via HAA with an H atom abstractor.

To further investigate and assess the reactivity of (TPP)Fe(NH_3)$_2$ for N_2 generation via a hydrazine pathway, we calculated the amide-amide coupling reaction to form a bridged hydrazido complex (**Figure 8**).

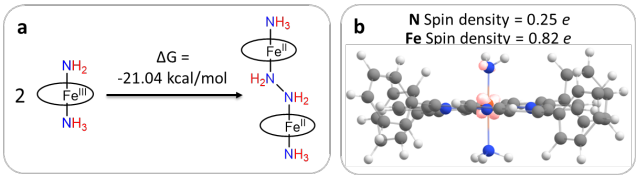

Figure 8: (a) Amide-amide coupling to form a bridged Fe^{II}-NH_2NH_2 complex, and (b) spin density (red surfaces; isovalue = 0.05) on the N and Fe atoms of the double spin state of (TPP)Fe(NH_3)(NH_2) prior to bimolecular coupling.

Amide-amide coupling for N-N bond formation is downhill in energy by 21.0 kcal/mol, which is 38.8 kcal/mol more favorable than the alternative HAA reaction to form the imido intermediate. Several studies have proposed aminyl character on M-NH_2 species can promote amide-amide coupling.[19, 21] Population analysis reveals a spin density of 0.25 *e* on the nitrogen atom of (TPP)Fe(NH_3)(NH_2). This is 0.20 *e* lower than that of (TMP)Ru(NH_3)(NH_2) (computed at the same level of theory), the postulated reactive intermediate for N-N bond formation in

our previous work on (TMP)Ru(NH_3)$_2$,[15] and 0.15 *e* lower than that of the Ni-NH_2 species (M06-L/def2-TZVP(Ni) and def2-SVP(all other atoms) level of theory) investigated by Peters and co-workers.[19] Hydrazine release followed by NH_3 adsorption on each Fe site to regenerate the starting (TPP)Fe(NH_3)$_2$ complex is 27.9 kcal/mol uphill in energy.

5. Conclusions

We used DFT to assess the reactivity of (TPP)M(NH_3)$_2$ complexes towards N-H bond cleavage and N-N bond formation for ammonia oxidation to dinitrogen. HAA from a single NH_3 molecule leading up to (TPP)M(NH_3)(N) is the most favorable pathway for all complexes except for (TPP)Ru(NH_3)$_2$ and (TPP)Os(NH_3)$_2$, which favor the formation of (TPP)M^{IV}(NH_2)$_2$ complexes. Trends in N-H BDFEs for a single NH_3 molecule resemble those previously calculated for (PY5)M complexes, suggesting that broad trends in reactivity towards N-H bond cleavage may be more metal-dependent for a metal in a nitrogen pseudo-octahedral environment. As observed for [(PY5)Mo(NH_3)]$^{2+}$ and [(PY5)W(NH_3)]$^{2+}$, (TPP)Mo(NH_3)$_2$ and (TPP)W(NH_3)$_2$ exhibit low and level N-H BDFEs due to a stabilized imide intermediate by multiple metal-ligand bonding.

Additionally, we investigated the reactivity of the (TPP)M(NH_3)$_2$ complexes towards N-N bond formation via NH_3 nucleophilic attack on imido and nitride intermediates. In the case of the Cr, Mn, Mo, and W porphyrin analogues, HAA to form the nitrido is favored over NH_3 nucleophilic attack on the imido. In the case of Fe, Co, and Ni, NH_3 nucleophilic attack on the imido intermediate followed by proton transfer to form a hydrazido intermediate is favored over nitride formation. Given the lower energetic cost to form the Fe imide intermediate compared to the Co and Ni analogues, we investigated further the N-N bond formation via a hydrazine pathway for (TPP)Fe(NH_3)$_2$, which has precedence in the literature to be a viable pathway towards N-N bond formation and N_2 generation. Our results suggest that Fe^{III}-•NH species with significant aminyl character can promote homolytic N-H bond cleavage of ammonia to form a Fe-NH_2 moiety and a transient •NH_2 radical that subsequently forms an N-N bond with the Fe-NH_2 moiety, bypassing the high energy requirement associated with NH_3 nucleophilic attack and proton transfer to form the hydrazido intermediate. Our results also indicate the need to inspect the radical character of Fe-imido species and their reactivity towards N-H bond cleavage of ammonia.

We additionally assessed the reactivity of the metalloporphyrins towards N-N bond formation via bimolecular coupling using the free energies associated with the release of N_2H_4, N_2H_2, and N_2 as proxies for the bimolecular reaction energies. Along with our work on [(PY5)M(NH_3)$_2$]$^{2+}$, our results demonstrate the need for an electrophilic M-N π bond for nitride-nitride coupling, provided that a nitride ligand can be formed electrochemically or via HAA with an H atom abstractor. Lastly, we investigated the reactivity of (TPP)Fe(NH_3)$_2$ to form a bridged hydrazido complex, and found bimolecular coupling of two Fe-amides for N-N bond formation to be 38.8 kcal/mol more favorable than further HAA to form the imido intermediate.

Ongoing work is focusing on investigating N-N bond formation via concerted NH_3 addition and N-H bond cleavage of NH_3 for the rest of the complexes, as well as bimolecular N-N coupling between (TPP)M(NH_3)(NH_x) intermediates. The present study and future investigation of N-N bond formation are essential to further unravel and optimize the reactivity of metalloporphyrins for ammonia oxidation.

Quantum mechanical methods

All DFT calculations for the present work were performed using ORCA 4.1.2.[40] The geometries of all structures were optimized in the gas phase using the B3LYP[41] exchange correlation functional with Grimme's D3 dispersion correction with Becke-Johnson damping.[42, 43] The 6-31G** basis set[44] for H, C, and N, and the def2-SVP[45] basis set for all transition metals along with associated effective core potential (ECP)[46] for second- and third-row transition metals were used. Standard state free energies were obtained from single point SMD solvation energies[47] in benzene, and thermal, entropic, and solvation contributions added to single point energies obtained using def2-TZVP[45] basis set on all atoms, as well as the associated ECP for second- and third-row transition metals.[46] Additional computational details of the DFT calculations can be found in section S1 of the supporting information.

A climbing-image Nudged Elastic Band (NEB-CI) calculation using 12 images as implemented in ORCA was performed to find the minimum energy path connecting the hydrogen-bonded (TPP)Fe(NH_3)(NH)--(NH_3) adduct and the hydrazido intermediate. This was followed by a saddlepoint-minimization using the default convergence criteria in ORCA.

Molecular Dynamics simulations

The local environment around the metalloporphyrins was explored with molecular dynamics simulations at 0.3 mM in liquid benzene saturated with ammonia ([NH_3] = 9.5 mM) to mimic as close as possible typical experimental conditions. MD simulations were performed using the Gromacs MD engine.[48] The porphyrin species were first solvated in a cubic box containg 513 benzene molecules and 20 NH_3 molecules. The system was minimized for 10 ps using the conjugate-gradient method then equilibrated in the NVE ensemble for 100 ps. The density of the system was allowed to equilibrate at constant pressure (1 atm) and temperature (298 K) in the NPT ensemble for 200 ps, and the box acquired dimensions of 4.3 x 4.3 x 4.3. A production run at constant pressure and temperature was done for 10 and 50 ns. The temperature was controlled with a stochastic thermostat[49] and the pressure was controlled with the extended Lagrangian-based Parrinello-Rahman barostat.[50] The integration timestep used in all simulations was 2 fs. The forcefield parameters for the MD simulations were taken from the Generalized Amber Force Field (GAFF) database,[51] and the parameters for the metal-nitrogen bonded interaction were taken from Abertí et al.[52]

Three 10 ns-long simulations were done to assess the interaction of the ammonia molecule and the solvent with the metalloporphyrins with different sets of charges. The first simulation used the Mulliken charges of the DFT optimized structure at the B3LYP/def2-SVP(metal) and 6-31G**(C, N, and H) level of theory using ORCA. The second simulation used the Mulliken charges of a single-point calculation of

the optimized structure using the def2-TZVP basis set for all atoms. The third simulation used RESP charges from a single point calculation of the ORCA-optimized geometry at the B3LYP/def2-TZVP level of theory in NWChem,[53] with that of the metal center constrained and obtained from NBO analysis at the same level of theory. Additional computational details of the MD simulations can be found in section S5 of the supporting information.

ASSOCIATED CONTENT

(Word Style "TE_Supporting_Information"). Supporting Information. A brief statement in nonsentence format listing the contents of material supplied as Supporting Information should be included, ending with "This material is available free of charge via the Internet at http://pubs.acs.org." For instructions on what should be included in the Supporting Information as well as how to prepare this material for publication, refer to the journal's Instructions for Authors.

AUTHOR INFORMATION

Corresponding Author

Simone.Raugei@pnnl.gov and Samanthajo.Johnson@pnnl.gov

Present Addresses

†If an author's address is different than the one given in the affiliation line, this information may be included here.

Author Contributions

The manuscript was written through contributions of all authors. All authors have given approval to the final version of the manuscript.

Notes

Any additional relevant notes should be placed here.

ACKNOWLEDGMENT

This work was supported as part of the Center for Molecular Electrocatalysis, an Energy Frontier Research Center funded by the U.S. Department of Energy, Office of Science, Office of Basic Energy Sciences. Computational resources were provided by the W. R. Wiley Environmental Molecular Sciences Laboratory (EMSL), a DOE National Scientific User Facility located at Pacific Northwest National Laboratory. M. M. M. would like to additionally thank the NNSA Minority Serving Institution Partnership Program (MSIPP) for funding.

ABBREVIATIONS

BDFE, bond dissociation free energy; HAA, hydrogen atom abstraction; DFT, density functional theory; MD, molecular dynamics; TPP, tetraphenylporphyrin; TMP, tetramesitylporphyrin; trpy, 2,2′:6′,2″-terpyridine; dmabpy, 4,4′-bis(dimethylamino)-2,2′- bipyridine; bpyPy$_2$Me, 6-(1,1-bis(pyridin-2-yl)ethyl)-2,2'-bipyridine; PY5, 2,6-bis(1,1-bis(2-pyridyl)ethyl)pyridine.

REFERENCES

(Word Style "TF_References_Section"). References are placed at the end of the manuscript. Authors are responsible for the accuracy and completeness of all references. Examples of the recommended formats for the various reference types can be found at http://pubs.acs.org/page/4authors/index.html. Detailed information on reference style can be found in The ACS Style Guide, available from Oxford Press.

ORCID

Melissa Barona: 0000-0001-7776-2677

SYNOPSIS TOC (Word Style "SN_Synopsis_TOC"). If you are submitting your paper to a journal that requires a synopsis graphic and/or synopsis paragraph, see the Instructions for Authors on the journal's homepage for a description of what needs to be provided and for the size requirements of the artwork.

To format double-column figures, schemes, charts, and tables, use the following instructions:

Place the insertion point where you want to change the number of columns
From the **Insert** menu, choose **Break**
Under **Sections**, choose **Continuous**
Make sure the insertion point is in the new section. From the **Format** menu, choose **Columns**
In the **Number of Columns** box, type **1**
Choose the **OK** button

Now your page is set up so that figures, schemes, charts, and tables can span two columns. These must appear at the top of the page. Be sure to add another section break after the table and change it back to two columns with a spacing of 0.33 in.

\Authors are required to submit a graphic entry for the Table of Contents (TOC) that, in conjunction with the manuscript title, should give the reader a representative idea of one of the following: A key structure, reaction, equation, concept, or theorem, etc., that is discussed in the manuscript. Consult the journal's Instructions for Authors for TOC graphic specifications.

Insert Table of Contents artwork here

---

1. Chehade, G.; Dincer, I., Progress in green ammonia production as potential carbon-free fuel. *Fuel* **2021,** *299*.
2. Elishav, O.; Mosevitzky Lis, B.; Miller, E. M.; Arent, D. J.; Valera-Medina, A.; Grinberg Dana, A.; Shter, G. E.; Grader, G. S., Progress and Prospective of Nitrogen-Based Alternative Fuels. *Chemical Reviews* **2020,** *120* (12), 5352-5436.
3. Chen, J. G.; Crooks, R. M.; Seefeldt, L. C.; Bren, K. L.; Bullock, R. M.; Darensbourg, M. Y.; Holland, P. L.; Hoffman, B.; Janik, M. J.; Jones, A. K.; Kanatzidis, M. G.; King, P.; Lancaster, K. M.; Lymar, S. V.; Pfromm, P.; Schneider, W. F.; Schrock, R. R., Beyond fossil fuel–driven nitrogen transformations. *Science* **2018,** *360* (6391).
4. Rees, N. V.; Compton, R. G., Carbon-free energy: a review of ammonia- and hydrazine-based electrochemical fuel cells. *Energy & Environmental Science* **2011,** *4* (4).
5. Schüth, F.; Palkovits, R.; Schlögl, R.; Su, D. S., Ammonia as a possible element in an energy infrastructure: catalysts for ammonia decomposition. *Energy Environ. Sci.* **2012,** *5* (4), 6278-6289.
6. Little, D. J.; Smith, I. I. I. M. R.; Hamann, T. W., Electrolysis of liquid ammonia for hydrogen generation. *Energy & Environmental Science* **2015,** *8* (9), 2775-2781.
7. Adli, N. M.; Zhang, H.; Mukherjee, S.; Wu, G., Review—Ammonia Oxidation Electrocatalysis for Hydrogen Generation and Fuel Cells. *Journal of The Electrochemical Society* **2018,** *165* (15), J3130-J3147.
8. Klerke, A.; Christensen, C. H.; Nørskov, J. K.; Vegge, T., Ammonia for hydrogen storage: challenges and opportunities. *Journal of Materials Chemistry* **2008,** *18* (20).
9. Liu, Y.; Meyer, T. J., Homogeneous catalysis for the nitrogen fuel cycle. *Proceedings of the National Academy of Sciences* **2019,** *116* (8), 2794-2795.
10. Weinberg, D. R.; Gagliardi, C. J.; Hull, J. F.; Murphy, C. F.; Kent, C. A.; Westlake, B. C.; Paul, A.; Ess, D. H.; McCafferty, D. G.; Meyer, T. J., Proton-Coupled Electron Transfer. *Chemical Reviews* **2012,** *112* (7), 4016-4093.

11. Bezdek, M. J.; Chirik, P. J., Interconversion of Molybdenum Imido and Amido Complexes by Proton-Coupled Electron Transfer. *Angewandte Chemie International Edition* **2018,** *57* (8), 2224-2228.
12. Margulieux, G. W.; Turner, Z. R.; Chirik, P. J., Synthesis and Ligand Modification Chemistry of a Molybdenum Dinitrogen Complex: Redox and Chemical Activity of a Bis(imino)pyridine Ligand. *Angewandte Chemie International Edition* **2014,** *53* (51), 14211-14215.
13. Bezdek, M. J.; Guo, S.; Chirik, P. J., Coordination-Induced Weakening of Ammonia, Water, and Hydrazine X–H Bonds in a Molybdenum Complex. *Science* **2016,** *354* (6313), 730-733.
14. Bhattacharya, P.; Heiden, Z. M.; Wiedner, E. S.; Raugei, S.; Piro, N. A.; Kassel, W. S.; Bullock, R. M.; Mock, M. T., Ammonia Oxidation by Abstraction of Three Hydrogen Atoms from a Mo–NH3 Complex. *Journal of the American Chemical Society* **2017,** *139* (8), 2916-2919.
15. Dunn, P. L.; Johnson, S. I.; Kaminsky, W.; Bullock, R. M., Diversion of Catalytic C–N Bond Formation to Catalytic Oxidation of NH3 through Modification of the Hydrogen Atom Abstractor. *Journal of the American Chemical Society* **2020,** *142* (7), 3361-3365.
16. Bhattacharya, P.; Heiden, Z. M.; Chambers, G. M.; Johnson, S. I.; Bullock, R. M.; Mock, M. T., Catalytic Ammonia Oxidation to Dinitrogen by Hydrogen Atom Abstraction. *Angewandte Chemie International Edition* **2019,** *58* (34), 11618-11624.
17. Warren, J. J.; Tronic, T. A.; Mayer, J. M., Thermochemistry of Proton-Coupled Electron Transfer Reagents and its Implications. *Chemical Reviews* **2010,** *110* (12), 6961-7001.
18. Johnson, S. I.; Heins, S. P.; Klug, C. M.; Wiedner, E. S.; Bullock, R. M.; Raugei, S., Design and reactivity of pentapyridyl metal complexes for ammonia oxidation. *Chemical Communications* **2019,** *55* (35), 5083-5086.
19. Gu, N. X.; Oyala, P. H.; Peters, J. C., Hydrazine Formation via Coupling of a Nickel(III)–NH 2 Radical. *Angewandte Chemie International Edition* **2020**.
20. Nakajima, K.; Toda, H.; Sakata, K.; Nishibayashi, Y., Ruthenium-catalysed oxidative conversion of ammonia into dinitrogen. *Nature Chemistry* **2019,** *11* (8), 702-709.
21. Nurdin, L.; Yang, Y.; Neate, P. G. N.; Piers, W. E.; Maron, L.; Neidig, M. L.; Lin, J.-B.; Gelfand, B. S., Activation of ammonia and hydrazine by electron rich Fe(ii) complexes supported by a dianionic pentadentate ligand platform through a common terminal Fe(iii) amido intermediate. *Chemical Science* **2021,** *12* (6), 2231-2241.
22. Collman, J. P.; Hutchison, J. E.; Ennis, M. S.; Lopez, M. A.; Guilard, R., Reduced nitrogen hydride complexes of a cofacial metallodiporphyrin and their oxidative interconversion. An analysis of ammonia oxidation and prospects for a dinitrogen electroreduction catalyst based on cofacial metallodiporphyrins. *Journal of the American Chemical Society* **1992,** *114* (21), 8074-8080.
23. Collman, J. P.; Hutchison, J. E.; Lopez, M. A.; Guilard, R., A stable dinitrogen complex of a ruthenium cofacial diporphyrin. *Journal of the American Chemical Society* **1992,** *114* (21), 8066-8073.
24. Man, W.-L.; Tang, T.-M.; Wong, T.-W.; Lau, T.-C.; Peng, S.-M.; Wong, W.-T., Highly Electrophilic (Salen)ruthenium(VI) Nitrido Complexes. *Journal of the American Chemical Society* **2004,** *126* (2), 478-479.
25. Coia, G. M.; Devenney, M.; White, P. S.; Meyer, T. J.; Wink, D. A., Osmium Hydrazido and Dinitrogen Complexes. *Inorganic Chemistry* **1997,** *36* (11), 2341-2351.
26. Coia, G. M.; White, P. S.; Meyer, T. J.; Wink, D. A.; Keefer, L. K.; Davis, W. M., Preparation of Osmium Hydrazido Complexes by Interception of an Osmium(IV) Imido Intermediate. *Journal of the American Chemical Society* **2002,** *116* (8), 3649-3650.
27. Habibzadeh, F.; Miller, S. L.; Hamann, T. W.; Smith, M. R., Homogeneous electrocatalytic oxidation of ammonia to N2 under mild conditions. *Proceedings of the National Academy of Sciences* **2019,** *116* (8), 2849-2853.

28. Najafian, A.; Cundari, T. R., Computational Mechanistic Study of Electro-Oxidation of Ammonia to N2 by Homogenous Ruthenium and Iron Complexes. *The Journal of Physical Chemistry A* **2019,** *123* (37), 7973-7982.
29. Zott, M. D.; Peters, J. C., Enhanced Ammonia Oxidation Catalysis by a Low-Spin Iron Complex Featuring Cis Coordination Sites. *Journal of the American Chemical Society* **2021,** *143* (20), 7612-7616.
30. Dunn, P. L.; Cook, B. J.; Johnson, S. I.; Appel, A. M.; Bullock, R. M., Oxidation of Ammonia with Molecular Complexes. *Journal of the American Chemical Society* **2020,** *142* (42), 17845-17858.
31. Dunn, P. L., Barona, M., Johnson, S. I., Raugei, S., and Bullock, R. M., Hydrogen Atom Abstraction from an OsII(NH3)2 Complex Gener-ates an OsIV(NH2)2 Complex: Experimental and Computational Analysis of the N-H Bond Dissociation Free Energies and Reactivity. *In preparation*.
32. Glendening, E. D.; Landis, C. R.; Weinhold, F., NBO 6.0: Natural bond orbital analysis program. *Journal of Computational Chemistry* **2013,** *34* (16), 1429-1437.
33. Nugent, W. A., Mayer, J. M., *Metal-Ligand Multiple Bonds*. Wiley Interscience: New York, 1988.
34. Zott, M. D.; Garrido-Barros, P.; Peters, J. C., Electrocatalytic Ammonia Oxidation Mediated by a Polypyridyl Iron Catalyst. *ACS Catalysis* **2019,** *9* (11), 10101-10108.
35. Suarez, A. I. O.; Lyaskovskyy, V.; Reek, J. N. H.; van der Vlugt, J. I.; de Bruin, B., Complexes with Nitrogen-Centered Radical Ligands: Classification, Spectroscopic Features, Reactivity, and Catalytic Applications. *Angewandte Chemie International Edition* **2013,** *52* (48), 12510-12529.
36. Mills, G.; Jónsson, H.; Schenter, G. K., Reversible work transition state theory: application to dissociative adsorption of hydrogen. *Surface Science* **1995,** *324* (2-3), 305-337.
37. Henkelman, G.; Jónsson, H., Improved tangent estimate in the nudged elastic band method for finding minimum energy paths and saddle points. *The Journal of Chemical Physics* **2000,** *113* (22), 9978-9985.
38. Eikey, R., Nitrido and imido transition metal complexes of Groups 6–8. *Coordination Chemistry Reviews* **2003,** *243* (1-2), 83-124.
39. Seymore, S. B.; Brown, S. N., Polar Effects in Nitride Coupling Reactions. *Inorganic Chemistry* **2002,** *41* (3), 462-469.
40. Neese, F.; Wennmohs, F.; Becker, U.; Riplinger, C., The ORCA quantum chemistry program package. *The Journal of Chemical Physics* **2020,** *152* (22).
41. Becke, A. D., Density-functional thermochemistry. III. The role of exact exchange. *The Journal of Chemical Physics* **1993,** *98* (7), 5648-5652.
42. Grimme, S.; Antony, J.; Ehrlich, S.; Krieg, H., A consistent and accurate ab initio parametrization of density functional dispersion correction (DFT-D) for the 94 elements H-Pu. *The Journal of Chemical Physics* **2010,** *132* (15).
43. Grimme, S.; Ehrlich, S.; Goerigk, L., Effect of the damping function in dispersion corrected density functional theory. *Journal of Computational Chemistry* **2011,** *32* (7), 1456-1465.
44. Hehre, W. J.; Ditchfield, R.; Pople, J. A., Self—Consistent Molecular Orbital Methods. XII. Further Extensions of Gaussian—Type Basis Sets for Use in Molecular Orbital Studies of Organic Molecules. *The Journal of Chemical Physics* **1972,** *56* (5), 2257-2261.
45. Weigend, F.; Ahlrichs, R., Balanced basis sets of split valence, triple zeta valence and quadruple zeta valence quality for H to Rn: Design and assessment of accuracy. *Physical Chemistry Chemical Physics* **2005,** *7* (18).
46. Andrae, D.; H**u**ermann, U.; Dolg, M.; Stoll, H.; Preu, H., Energy-adjustedab initio pseudopotentials for the second and third row transition elements. *Theoretica Chimica Acta* **1990,** *77* (2), 123-141.

47. Marenich, A. V.; Cramer, C. J.; Truhlar, D. G., Universal Solvation Model Based on Solute Electron Density and on a Continuum Model of the Solvent Defined by the Bulk Dielectric Constant and Atomic Surface Tensions. *The Journal of Physical Chemistry B* **2009,** *113* (18), 6378-6396.
48. Abraham, M. J.; Murtola, T.; Schulz, R.; Páll, S.; Smith, J. C.; Hess, B.; Lindahl, E., GROMACS: High performance molecular simulations through multi-level parallelism from laptops to supercomputers. *SoftwareX* **2015,** *1-2*, 19-25.
49. Bussi, G.; Donadio, D.; Parrinello, M., Canonical sampling through velocity rescaling. *The Journal of Chemical Physics* **2007,** *126* (1).
50. Parrinello, M.; Rahman, A., Polymorphic transitions in single crystals: A new molecular dynamics method. *Journal of Applied Physics* **1981,** *52* (12), 7182-7190.
51. Cornell, W. D.; Cieplak, P.; Bayly, C. I.; Gould, I. R.; Merz, K. M.; Ferguson, D. M.; Spellmeyer, D. C.; Fox, T.; Caldwell, J. W.; Kollman, P. A., A Second Generation Force Field for the Simulation of Proteins, Nucleic Acids, and Organic Molecules. *Journal of the American Chemical Society* **2002,** *117* (19), 5179-5197.
52. Albertí, M.; Amat, A.; Farrera, L.; Pirani, F., From the (NH3)2–5 clusters to liquid ammonia: Molecular dynamics simulations using the NVE and NpT ensembles. *Journal of Molecular Liquids* **2015,** *212*, 307-315.
53. Valiev, M.; Bylaska, E. J.; Govind, N.; Kowalski, K.; Straatsma, T. P.; Van Dam, H. J. J.; Wang, D.; Nieplocha, J.; Apra, E.; Windus, T. L.; de Jong, W. A., NWChem: A comprehensive and scalable open-source solution for large scale molecular simulations. *Computer Physics Communications* **2010,** *181* (9), 1477-1489.